Surface & Coatings Technology 205 (2011) 3211–3217

Contents lists available at ScienceDirect

Surface & Coatings Technology

journal homepage: www.elsevier.com/locate/surfcoat

Direct measurement of strain behavior of compression loaded plasma-sprayed yttria-stabilized zirconia

Christopher Petorak, Rodney W. Trice *

Purdue University, School of Materials Engineering, West Lafayette, IN 47907, United States

ARTICLE INFO

Article history:
Received 30 July 2010
Accepted in revised form 16 November 2010
Available online 24 November 2010

Keywords:
Thermal barrier coatings
YSZ
Mechanical properties
Anelasticity
Strain tolerance

ABSTRACT

Direct measurement of the stress–strain behavior of stand-alone plasma-sprayed 7 wt.% Y_2O_3–ZrO_2 (YSZ) coatings was made at room temperature. YSZ coatings were evaluated in the as-sprayed condition, and after heat-treatments for 10, 50, and 100 h at 1200 °C using both monotonic and two different cyclic uniaxial compression loading profiles. Heat-treatments were used to change the primarily mechanically interlocked system of lamella to a chemical interlocked system. Monotonic loading of the coatings indicated three different moduli. The first modulus was lower (~10 GPa) than observed typically in a plasma sprayed coating. The relatively easy deformation associated with the low modulus was attributed to minor sample crushing near its ends. The second modulus observed was ~24 GPa and is due to closure of cracks oriented perpendicular to the stress and lamella sliding and compaction. The third modulus measured ranged from 40 to 48 GPa and represents the elasticity of the material after the easy crack closure and lamella sliding events have occurred. In repeated cyclic loading to a compressive stress of 60 MPa, the coatings were observed to demonstrate large amounts of non-recoverable strain during the first several load/unload cycles, presumably due to permanent sliding and compaction of lamella. Permanent strain tended to a minimum amount after ~20 load/unload cycles. Increased cyclic loading from 20 to 320 MPa in 20 MPa increments revealed significant anelastic behavior as evidenced by stress–strain hysteresis loops, particularly in the as-sprayed coating. The elastic moduli of the coatings upon reloading were observed to increase after each subsequent 20 MPa increase in stress applied to the coating to values as high as ~80 GPa. This was attributed to an increase in the volume fraction of coating sustaining the load. The amount of non-recoverable strain was highest in the heat-treated coatings indicating a loss of strain tolerance of YSZ coatings during simulated service conditions.

© 2010 Elsevier B.V. All rights reserved.

1. Introduction

Atmospheric or air plasma-sprayed (APS) coatings are formed by the impingement and subsequent stacking of melted droplets on a substrate [1–4]. The unique and complex microstructure formed as a result of APS comprised two primary defects that, to a first approximation, are oriented orthogonal to each other [5,6]. These defects include (1) highly elongated pores that exist between the long axis of the stacked lamella (i.e. deemed interlamellar porosity) and within the plane of the coating, and (2) intralamellar cracks that tend to cut through the lamella and are oriented perpendicular to the coating plane. Coatings with less porosity and vertical cracks that extend through the thickness of the coatings (i.e. segmented cracks) can also be produced by increasing the power (and therefore the temperature) during spraying [7–9]. Thermal barrier coatings or TBCs, like those made from APS 7 wt.% Y_2O_3–ZrO_2 or YSZ, employ these defects to lower thermal conductivity and increase strain tolerance.

Plasma-sprayed coatings are a uniquely interlocked system of lamellae splats that do not display all characteristic behaviors of a dense solid ceramic [10,11]. Deformation behavior for APS YSZ at room temperature has been attributed to mechanisms such as intralamellar crack closure perpendicular to the applied load, opening of favorably oriented intralamellar cracks, and lamella sliding [12–16]. As discussed in several recent papers [17,18], the intralamellar cracks are believed to cause the anelastic mechanical behavior observed in thermally sprayed coatings. Anelasticity is defined as a non-linear elastic response of a material, particularly evident in hysteresis loops during mechanical loading and unloading. It is believed that the intralamellar cracks oriented approximately perpendicular to the applied stress contribute primarily to anelastic behavior such that an in-plane compressive stress, like those that occur during service conditions, will first tend to close parts of the crack. With subsequent increases in stress, the previously closed crack face can slip or become unstuck relative to one another as the friction between the two surfaces is overcome. Upon unloading, the crack faces can slide back to

* Corresponding author. Tel.: +1 765 494 6405.
E-mail address: rtrice@purdue.edu (R.W. Trice).

0257-8972/$ – see front matter © 2010 Elsevier B.V. All rights reserved.
doi:10.1016/j.surfcoat.2010.11.041

their prior position and the previously closed crack can open. If this scenario was all that occurred within the microstructure of the coating, then no permanent strain would be observed. However, in-situ observation of crack behavior in stand-alone APS YSZ at 25 °C revealed that cracks oriented between 30 and 60° with respect to the loading axis will nucleate new cracks that propagate parallel to the applied stress [14]. Thus, while there are elastic-deformation mechanisms (crack closure and relative sliding of faces), there are also permanent deformation mechanisms (initiation and growth of new cracks). Other mechanisms that impart permanent strains may also be possible at room temperature, including compaction of the lamella as reported currently.

The current study characterizes the room temperature deformation behavior of stand-alone APS YSZ. Knowing that TBCs are used at high temperature, the focus presently is not to simply characterize the deformation behavior at room temperature, but also to differentiate deformation mechanisms occurring at room temperature where contributions from diffusion-based deformation mechanisms (like creep) are negligible. The knowledge of plasma-sprayed compressive deformation gained at room temperature can then be applied to the more complex high-temperature scenarios. All tests were performed on stand-alone coatings in compression, affording isolation of the mechanical behavior of the coating without requiring compensation for the underlying substrate. This will afford direct measurement of the anelastic properties of plasma-sprayed YSZ.

Several different compressive loading scenarios and coating conditions were employed to help differentiate between dominant deformation mechanisms. Coatings in the as-sprayed condition and after heat treatments at 1200 °C were investigated. As a coating is exposed to temperatures experienced in-service (1100 °C or greater), the initially mechanical interlocked system of lamellae splats changes to a chemically bonded microstructure as sintering necks form between areas of adjacent lamella contact [1,5,19–21] with a loss of interlamellar porosity observed. Erk et al. [22] applied Mullin's thermal grooving analysis [23,24], to APS YSZ and found densifying bulk diffusion to be the dominant mass transport mechanism above 1100 °C. Chemical bonding between lamellae would be expected to change the mechanical response of the coating.

Of particular interest in this paper is the loss of strain tolerance as a result of repeated stress application and heat-treatment. It is well established that during service TBC coatings are initially in compression during engine heat-up [25]. During engine cool down, the stress state in the coating reverses to tension and the amount of permanent compressive deformation will determine the magnitude of the tensile stress. The trend is that more permanent compressive deformation causes a high tensile stress in the coating, an unfavorable condition for the ceramic coating that can cause large thru-thickness cracks and coating delamination. Thus, coatings with a high degree of elastic strain tolerance are desired. Heat-treatment of the coating can change the strain tolerance of the coating, converting the mechanically interlinked coating of lamella to chemically bonded lamella.

2. Experimental procedure

2.1. Fabrication of stand-alone YSZ coatings

Air plasma-sprayed stand-alone coatings were utilized for all mechanical tests, and were produced in accordance with the parameters and methods outlined in previous work [26–28], and are briefly reviewed here. The coatings were comprised a fused and crushed HC-Starck Amperit 825.0 7 wt.% Y_2O_3–ZrO_2 powder having a particle size of 22.5 ± 6 μm and were sprayed at Ames Laboratory using a Praxair SG-100 gun with a 730 anode (part number), a 729 cathode and a 113 gas injector. Cylindrical copper rods (12.7 mm in diameter and 250 mm long) served as the substrate for the coatings. Generally, 40 cycles of vertical strokes were applied as the substrate was rotated; a stroke equals one pass down and one pass up of the SG-100 gun. The coatings were nominally ~0.6 mm thick, with specific coating thicknesses used to calculate the stress for each sample. The spray conditions are listed in Table 1.

Table 1
Thermal spray conditions used for fabrication of YSZ coatings.

Power	37 kW
Stand-off distance	10 cm
Arc gas rate	25 slm (Ar)
Aux gas rate	21 slm (He)
Powder carrier gas rate	6 slm (Ar)

The samples were sectioned into ~18 mm lengths. To produce stand-alone coatings, the copper substrates were removed by etching the YSZ coatings with nitric acid. The coatings were subsequently cleaned using acetone and height and coating thickness were measured using calipers. The coatings were all mechanically evaluated at room temperature in either the as-sprayed condition or after heat-treating. Heat-treatment conditions included 10, 50 or 100 h at 1200 °C. Density of the coatings was measured using Archimedes technique using a theoretical density of 6.08 g/cm^3 for YSZ [29]. The total standard deviation was calculated from both the uncertainty of a repeated measurement on the same sample, and the deviation for a pooled group of coatings. For example, the as-sprayed condition had an established uncertainty of 0.09 g/cm^3, and a standard deviation between replicates of ± 0.11 g/cm^3, which resulted in the total standard deviation of ± 0.14 g/cm^3.

2.2. Mechanical testing of stand-alone YSZ coatings

2.2.1. Testing overview

Uniaxial compression tests were performed at room temperature on stand-alone coatings. All testing on stand-alone coating samples was performed using a servo-hydraulic load frame (MTS 810 Load Frame) equipped with hydraulic collet grips, an alignment fixture (MTS609 Alignment Fixture), a 100 kN force transducer, and SiC pushrods. Strain was measured with a rod-type extensometer (MTS 632.70H-01) with a resolution of ± 1 μm. Alignment of the load train was performed prior to testing. Force was directly measured using the 100 kN load transducer with an accuracy of ± 1.5 N established. Data was monitored using the MTS-TestStar and TestWare-SX Model 790.00 Version 4.0D software at a rate of 0.25/s for compression tests.

Three loading profiles were used to investigate the properties of stand-alone YSZ coatings at room-temperature. These profiles include: 1) monotonic loading, 2) increased-load cyclic testing, and 3) constant-load cyclic testing. All profiles applied the compressive load at a rate of 20 N/s.

2.2.2. Monotonic uniaxial compression testing

The monotonic loading profile applied a compressive load to the sample until failure. Monotonic loading was performed to establish the uniaxial compression modulus, E, of the as-sprayed and heat-treated coatings. The compliance of the load frame was accounted for in these measurements.

2.2.3. Cyclic uniaxial compression testing

The coatings were loaded in two cyclic stress profiles, constant-load cyclic testing and increased-load cyclic testing, to gain insight in the nature of strain accommodation in APS YSZ coatings. A constant-load cyclic testing profile simply cycled 41 times between 20 and 60 MPa. Sixty megapascals was chosen as it represents a stress that would not normally fail a stand-alone coating. Constant-cyclic loading was performed on 10 h/1200 °C and 50 h/1200 °C heat-treated coatings.

The increased-load cyclic profile applied an increasingly larger compressive stress to a designated maximum stress, then unloaded to 20 MPa, and reloaded again 20 MPa *past* the previous maximum

stress. For example, a sample would first be loaded to a compressive stress of 40 MPa, then unloaded to 20 MPa, reloaded again to 60 MPa, unloaded to 20 MPa, etc. A minimum unload stress of 20 MPa was chosen to keep the platen and the sample in contact during testing. The samples were typically stressed to ~320 MPa prior to failure.

For either cyclic loading testing profiles the compliance of the load frame was not removed due to the increased complexities of the data set. Thus, relative modulus values will be denoted "m" for the slope of the linear curve fit in contrast to "E" used for monotonic loading data where the compliance of the load frame was subtracted.

The permanent strain for either cyclic loading profile types was calculated for each cycle by subtracting the strain values that correlated to the minimum stress value, i.e. 20 MPa, of each unload cycle, denoted by $e_{20\ MPa}$. The permanent strain-per-cycle can be mathematically represented as:

$$\text{Permanent Strain}_{(n+1)} = \left[e_{20\,MPa_{(n+1)}} - e_{20\,MPa_{(n)}}\right] \quad (1)$$

where n corresponds to the cycle . The recoverable strain-per-cycle was calculated by subtracting the non-recoverable strain-per-cycle from the total strain-per-cycle, which was taken to be the strain at the point of maximum load, denoted by e_{max}. The recoverable strain-per-cycle can be mathematically expressed as:

$$\text{Recoverable Strain}_{(n+1)} = e_{max_{(n)}} - \left[e_{20\,MPa_{(n+1)}} - e_{20\,MPa_{(n)}}\right]. \quad (2)$$

3. Results and discussion

3.1. Coating properties

The bulk density, open, closed and total porosity, and the number of samples characterized for each measurement are provided for the as-sprayed and heat-treated conditions in Table 2. The bulk density of the coatings heat-treated at 1200 °C did not statistically change when compared to the as-sprayed coatings. However, the coatings heat-treated at 1200 °C did display an increase in the amount of open porosity and a decreased amount of closed porosity relative to the as-sprayed coatings. For example, the change in open porosity observed between as-sprayed and heat-treated coatings for the shortest time of 10 h/1200 °C was 3.5%, which is a measurable change within the established open porosity uncertainty of ±0.65% as determined by a Gaussian law of error propagation.

3.2. Monotonic compressive loading of stand-alone coatings

An example of a monotonically loaded sample is provided in Fig. 1 for a stand-alone sample heat-treated for 50 h at 1200 °C. E_{crush} is defined as the initial elastic modulus observed, and was a characteristic of some mechanical crushing near the ends of the coating and was visibly verified by powder remnant on the platens after the coatings were removed. Less crushing was noted for the heat-treated samples tested at room temperature than as-sprayed samples. The initial low modulus E_{crush} region was followed by an observed increase in elastic modulus, and if failure did not occur, a second increase in modulus. The first and second increases in modulus are referred to as E_{o1} and E_{o2}, respectively, as indicated in Fig. 1. Coatings in the current study transitioned to the E_{o2} modulus between 0.8 and 1.2% strain.

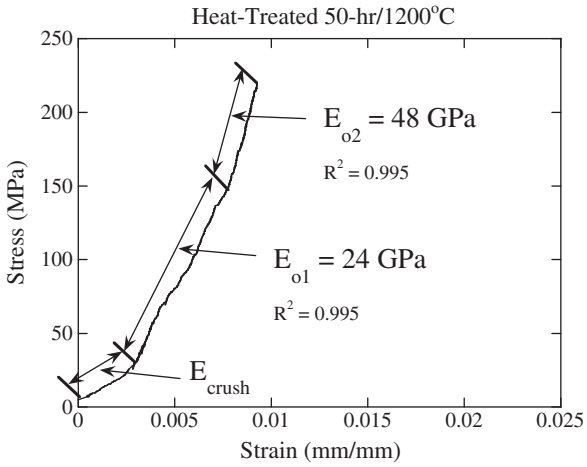

Fig. 1. Monotonic stress–strain response at room temperature for a 50 h/1200 °C heat-treated plasma-sprayed coating. As-sprayed coating and those heat-treated for 10 and 100 h at 1200 °C also demonstrated similar behavior. Heat treated coatings exhibited some auditory and visual cracking events in these generally stiffer coatings.

The elastic moduli measured for the monotonically loaded coating in various conditions are presented in Table 3. In general, note that E_{crush} displays a very low modulus of 8–10 GPa, independent of coating condition. E_{o1} ranges between 22 and 27 GPa and E_{o2} ranges from 40 to 48 GPa. Exact modulus values for the 10 h/1200 °C heat-treated coating were difficult to accurately assess because of the great number of inflections caused by a number of cracking events. The 10 h/1200 °C heat-treated coatings failed prior to the onset of the second loading modulus, E_{o2}. Not enough samples were tested to statistically assert differences in moduli as a result of heat-treatments. Dense YSZ has a modulus range between 196 and 217 GPa [30]. This value decreases to approximately 20–40 GPa for plasma-sprayed coating [31–34], values similar to those measured presently.

E_{o1} and E_{o2} are believed to be linked with the macroscopic mechanical behavior of the plasma-sprayed microstructure. Previous work by Thompson and Clyne [35] predicted an increase in the modulus of APS YSZ at ≈1% strain due to 1) elastic closure of intralamellar cracks oriented perpendicular to the applied load, and 2) inhibited shear-induced lamella sliding. These mechanisms are believed to determine E_{o1} and the transition to E_{o2} observed in the current data set. Below the ≈1% strain level the majority of crack faces perpendicular to the applied compressive load are in the *process* of closing, bringing the upper and lower crack faces in contact, which absorbs strain energy elastically. Levin et al. [14] directly observed crack closure via in-situ compression experiments on plasma-sprayed YSZ coatings in the E_{o1} region. In addition to elastic mechanisms, an effective densification of the coating is thought to occur in the E_{o1} region in the form of lamellae and crack face sliding, where uninhibited or loosely mechanically bound splats are sliding past

Table 2
Average physical properties of the as-sprayed and heat-treated stand-alone coatings of YSZ.

Property	As-sprayed	10 h/1200 °C	50 h/1200 °C	100 h/1200 °C
Bulk density (g/cm^3)	5.52 ± 0.14	5.55 ± 0.13	5.54 ± 0.14	5.60 ± 0.12
Open porosity (%)	2.3 ± 1.4	5.8 ± 0.9	5.3 ± 0.7	4.9 ± 0.6
Closed porosity (%)	7.1 ± 2.8	3.0 ± 2.3	3.7 ± 2.4	3.2 ± 2.1
Total porosity (%)	9.4 ± 2.3	8.8 ± 2.2	9.0 ± 2.4	8.1 ± 1.9
Number samples	95	24	21	6

Table 3
Modulus data generated by linear curve fit for as-sprayed and heat-treated coatings monotonically loaded in compression at room temperature. An "X" denotes that a modulus was not able to be determined due to coating failure.

Coating condition	$E_{crushing}$ (GPa)	E_{o1} (GPa)	E_{o2} (GPa)
As-sprayed	10 ± 2	22 ± 3	40
10 h/1200 °C	10	27	X
50 h/1200 °C	8	24	48

one another until becoming locked in place by neighboring lamella [35].

Above the approximately 1% strain value at room temperature the majority of perpendicular crack faces are now in contact, resulting in a more uniformly distributed load throughout the volume of plasma-sprayed material. Levin [14] directly observed that crack closure of ~0.2 μm was observed to cause an increase in modulus similar to the E_{o2} region observed presently. The mechanisms that lead to increased modulus are counter-acted by the opening and formation of cracks that would tend to reduce the modulus in the coatings. Levin noted that cracks oriented parallel to the loading direction were found to open ≈0.4–0.5 μm as a result of the applied stress [14]. New cracks also formed during loading; these cracks were oriented 30–60° off-axis with respect to the load direction. Ultimately, catastrophic failure occurs by crack linkage parallel to the applied load during compressive loading [10,11,36]. In the current study it was not uncommon for a failed coating to display individual columns of coating that had become completely detached from the rest of the sample.

3.3. Constant-cyclic compressive loading of stand-alone coatings at room temperature

Constant-stress cyclic deformation experiments on stand-alone YSZ coatings provide insight into the effect of repeated stress loadings on strain accommodation of heat-treated coatings. The characteristic stress versus strain behavior for the 10 h/1200 °C for up to 41 cycles between 20 and 60 MPa is shown in Fig. 2. Prior to reaching 60 MPa associated with the first cycle, it was noted that when the previously applied maximum applied stress of 40 MPa was surpassed the modulus decreased substantially from 53 to 20 GPa. This sharp transition in apparent modulus was attributed to the lamella sliding events. Similar characteristic results were obtained for coatings that are constantly cyclically tested at room temperature after a 50 h/1200 °C heat-treatment.

The cyclic stress results will generally be addressed with respect to two distinct coating behaviors: 1) the pristine stress–strain behavior, which is denoted 'm_{o1}' (analogous to E_{o1}, but without the load frame compliance removed), and 2) the unloading/reloading curve. The pristine stress–strain behavior is the coating response the first time it is loaded. Each unloading/reloading curve displays a very narrow linear hysteresis loop suggesting elastic deformation primarily contributes, and therefore the unloading/reloading slope of the stress strain curves will be denoted '$m_{e\#}$.' The subscript 'e' stands for elastic and the subscript '#' represents the cycle number from 1 to 41.

As shown in Fig. 2, the slopes of the unloading and the reloading behavior between 20 and 60 MPa indicate no difference in relative modulus between the first reload ($m_{e1} = 59$ GPa) and the forty-first reload ($m_{e41} = 60$ GPa). The amount of permanent strain caused by each loading cycle is presented in Fig. 3 for coatings heat treated at 1200 °C for either 10 or 50 h. As shown in Fig. 3, the amount of permanent strain is higher initially in the coating heat-treated for only 10 h at 1200 °C, consistent with less time to establish chemical bonding between the lamella than for a 50 h/1200 °C heat treatment. Thus, it appears that as the lamella became more chemically attached via diffusion, the amount of strain tolerance is decreased.

The largest amount of permanent strain occurs during the first few cycles of the experiment. However, small amounts of permanent deformation continue to take place during constant stress cycling, even though the reloading/unloading modulus, m_e, does not change. Fig. 3 shows that as the number of reload cycles increases, the amount of non-recoverable strain tends toward 1×10^{-5} mm/mm, independent of heat-treatment. The physical significance of this saturation is not completely understood. It is not unreasonable to consider lamella sliding or shifting to redistribute the stress more uniformly in the arguments proposed. The assumption must be made that 100% of the volume of the material does *not* bear the load initially, and that through lamella rearrangement a greater and greater percent of material will come to bear the total applied load. Perhaps after ~40 load/unload cycles the best packing of loosely bonded lamellae has been achieved for the magnitude of the applied load and therefore a plateau is reached. Application of larger maximum loads would result in the possibility of again shifting stuck adjacent lamellae to continually redistribute the load.

3.4. Increased-cyclic uniaxial compressive loading of stand-alone coatings

The results of coatings tested using an increased-cyclic loading profile are shown in Fig. 4a–c for samples tested at room temperature in the as-sprayed condition, and after 1200 °C heat-treatments for 10 and 100 h, respectively. Note that the reloading data (defined as from 20 MPa to the prior maximum applied stress) follows the same basic path as the unloading data evidenced by small hysteresis loops. This

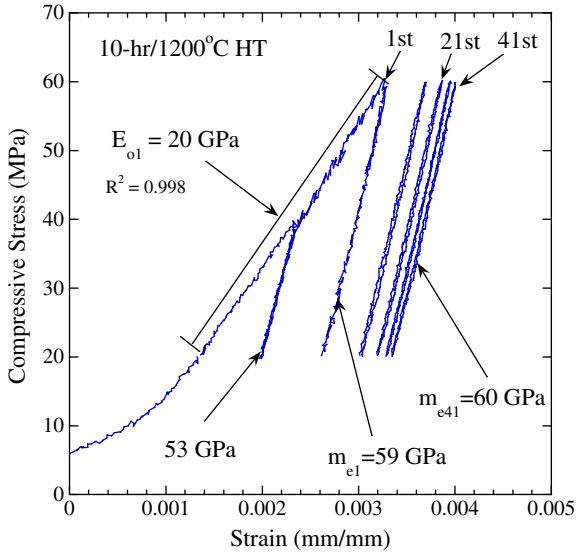

Fig. 2. Stress/strain response for a stand-alone coating heat-treated at 1200 °C for 10 h and then repeatedly compressed between 20 and 60 MPa at 25 °C. Note only the 1st, 11th, 21st, 31st and 41st 20–60 MPa cycles are shown to distinguish the stress/strain trend for repeated compressive cycling at the same stress level. The loading cycle to 40 MPa was not the first cycle; rather only cycles to 60 MPa were enumerated 1 through 41.

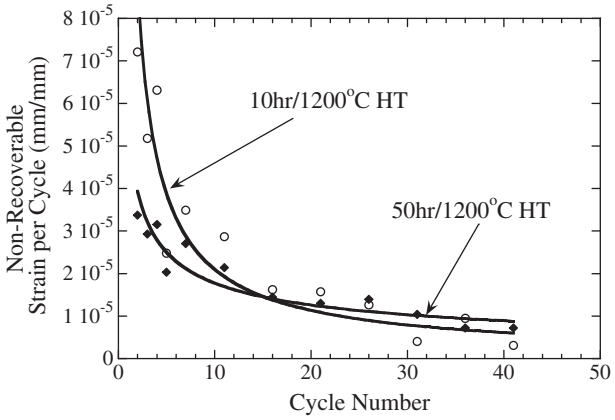

Fig. 3. Plot of the non-recoverable strain for each cycle during constant-cycling through the 41st cycle. Note that with repeated stress application to 60 MPa, the amount of permanent strain decreases in magnitude.

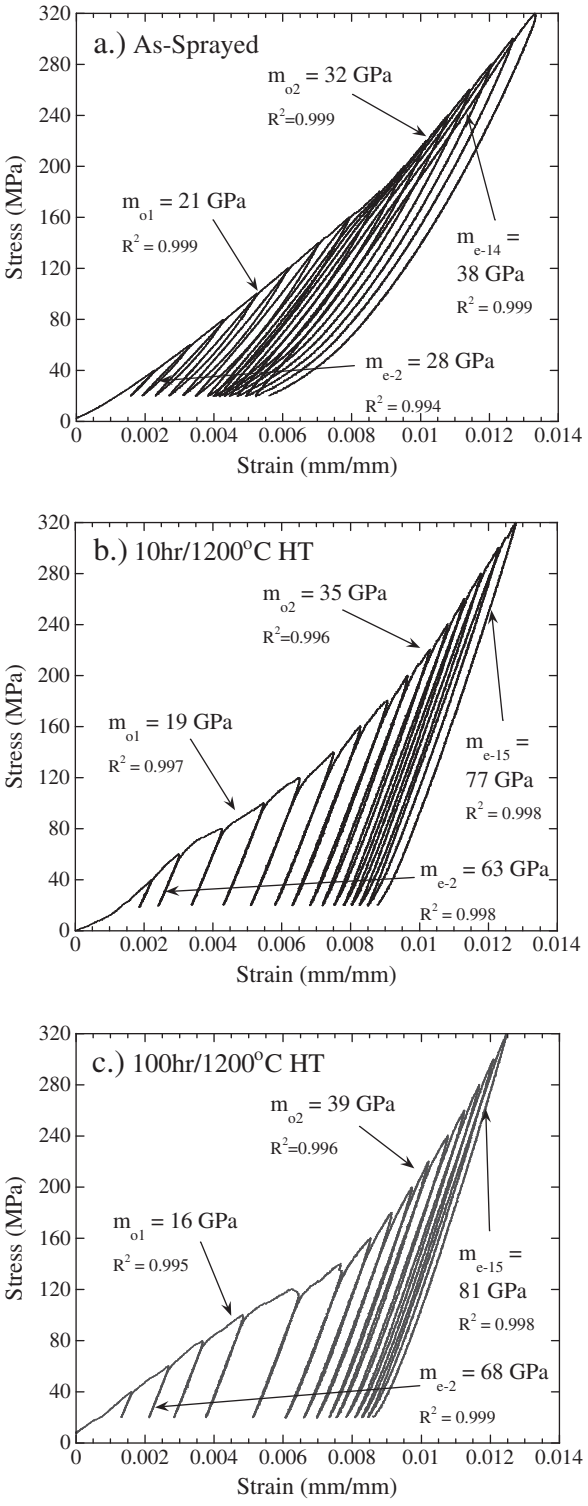

Fig. 4. Stress–strain response for an increasing-cyclic loading profile of a stand-alone coating in the (a) as-sprayed condition, and after (b) 10 h and (c) 100 h at 1200 °C, then compressively cycled at 25 °C.

behavior is particularly evident in the heat-treated coatings (Fig. 4b and c) indicating that strain can be accommodated without new cracks either nucleating or growing until it surpasses the prior maximum stress. The reloading/unloading curve is designated $m_{e-\#}$, where # is the cycle number from 1 to 15. For example, the loading/unloading cycle associated with a stress of 20 to 320 MPa is designated m_{e-15}.

The application of a new initial larger stress, capable of propagating new cracks and major lamella sliding events, results in a new decreased relative loading modulus, which is designated m_{ox}, where x is designated as 1 prior to the increase in loading modulus and 2 after the increase. All of the increased-cyclically loaded coatings display an increase in relative loading modulus, m_{o1} to m_{o2}, which was observed in coatings during monotonic loading. The m_{ox} values for each coating condition subjected to increased-cyclically loading conditions are displayed in Table 4. The increase in relative modulus occurs in roughly the same stress range of approximately 140–160 MPa for all coating heat-treatment conditions (i.e. 10, 50, or 100 h at 1200 °C).

There are two important observations with regard to Fig. 4a, b, and c. First, with each additional loading cycle, i.e. increased amounts of permanent strain are imparted in the coating, the magnitude of $m_{e-\#}$ increases. Second, the amount of non-recoverable strain shows a distinct pattern for all plasma-spray coating conditions. These two observations are discussed in further detail below.

3.4.1. Effect of cyclic loading on coating volume sustaining the load

An assertion was made in Section 3.3 that 100% of the coating volume of the material does *not* bear the load initially, and that through lamella rearrangement a greater and greater percent of material will come to bear the total applied load. This assertion is considered in greater detail presently using a simple energy/volume analysis of the reloading stress–strain data from 20 to 40 MPa for each cycle. The approach was to compare each reload cycle, understanding that with each cycle an increase of permanent deformation took place prior to the subsequent reloading.

The area under an elastic loading curve is equivalent to the energy per unit volume of the material ($W_{elastic}$) bearing the load per cycle and is given as:

$$W_{elastic} = \frac{1}{2}\Delta\sigma\Delta e = \frac{1}{2}\frac{\Delta F}{A}\frac{\Delta l}{l_o} = \frac{1}{2}\frac{\Delta F \Delta l}{V} \quad (3)$$

where $\Delta\sigma$ is the stress change over the desired interval of each reload curve, Δe is the change in strain resulting from the applied stress, ΔF is the change in force over the desired interval, Δl is the change in the length of the sample as measured using the extensometer, A is the cross-sectional area of the coating, l_o is the original height of the coating cylinder, and V is the volume of the coating sustaining the load.

$W_{elastic}$ was calculated for each reload cycle, 1 through 15, from the data represented in Fig. 4a–c. The stress increment considered was 20 to 40 MPa for each cycle. $W_{elastic}$ was noted to decrease from cycle 1 to 2, from cycle 2 to 3, etc. With consideration to the equation presented eqn. 3, the change in force for each reload cycle is constant because the loading rate is constant at 20 N/s. Thus, the observed decrease in $W_{elastic}$ for each sequential reload cycle is either due to a decrease in Δl or increase in the volume of material sustaining the load, V. It is argued here that the decrease in Δl noted for each reload cycle is due to the increase in the volume of the material carrying the load and that

Table 4
Relative loading modulus values for increased-cyclic loading profiles determined by linear curve fits.

Increased-cyclic loading	m_{o1} (GPa)	m_{o2} (GPa)
As-sprayed	21	32
10 h/1200 °C	19	35
50 h/1200 °C	24	42
100 h/1200 °C	16	39

this is a consequence of the deformation imparted to the material during the previous loading cycle. With this in mind, the percentage decrease in energy/volume was calculated by finding the difference in $W_{elastic}$ from one run to the next sequential run and is given by:

$$\%\text{Decrease in}\,W_{Elastic}\,\text{for Each Cycle}_{(n+1)} = \left|\frac{W_{Elastic(n+1)} - W_{Elastic(n)}}{W_{Elastic(n)}}\right| \times 100 \quad (4)$$

where n is a cycle number ranging from 1 up to 15. The cumulative decrease in $W_{elastic}$ for each increased-cyclic loading cycle is shown in Fig. 5 for the as-sprayed and heat-treated conditions. In general, there is a larger decrease in $W_{elastic}$ in the early unload/reload cycles (i.e. cycles 1 to 2, 2 to 3, etc.) compared to the later cycles (i.e. cycles 7 to 8, 9 to 10, etc.). Above ≈140 MPa $W_{elastic}$ continues to decrease, but at a slower rate. Note that all four coating conditions exhibit a cumulative decrease in $W_{elastic}$ of 22–29% just prior to failure of the coating.

It could be argued that crack growth decreased as the load became more uniformly distributed in the plasma-sprayed microstructure, and hence it is the dominant and only permanent deformation mechanism contributing during the entire loading cycle. But, an increase in m_e was observed during increased-cyclic loading, which would not be a consequence of parallel crack growth. If crack growth parallel to the applied compressive load was acting as the sole permanent deformation mechanism, the reloading modulus m_e would have to remain constant or decrease. There must be a second permanent deformation mechanism contributing during m_{o1} and m_{o2}. The proposed deformation mechanism is compaction of interlamellar pores, and rearrangement through lamella sliding. The compaction is further supported by the permanent changes in height of approximately 0.18 ± 0.04 mm for all coatings measured after increased-cyclic loading at room-temperature.

In summary, at the onset of testing the greatest volume fraction of favorably oriented and most loosely bound lamella are present. Compressive loads are applied and the strain is accommodated by loosely bound lamellae breaking free and sliding into more favorable locations, where the load is now redistributed to a larger fraction of the material. Note that adjacent lamella could have previously been frictionally stuck or chemically bonded (due to the heat-treatment). As the loading continues, more of the coating is bearing the compressive load, and fewer and fewer localized stresses exceed the frictional stresses between lamellae or fracture strength between lamellae of the material. Continued loading will propagate and link cracks perpendicular to the applied load, which will eventually result in catastrophic failure.

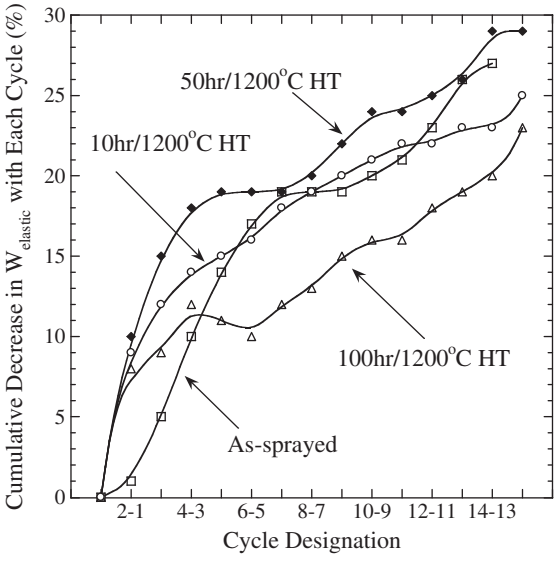

Fig. 5. Cumulative decrease in $W_{elastic}$ per cycle calculated from the elastic unloading/reloading curves of Fig. 4a, b, and c. The decrease in $W_{elastic}$ is believed to be due to the increase in volume sustaining the load as a function of lamella re-arrangement. The line for each coating condition is added to guide the eyes.

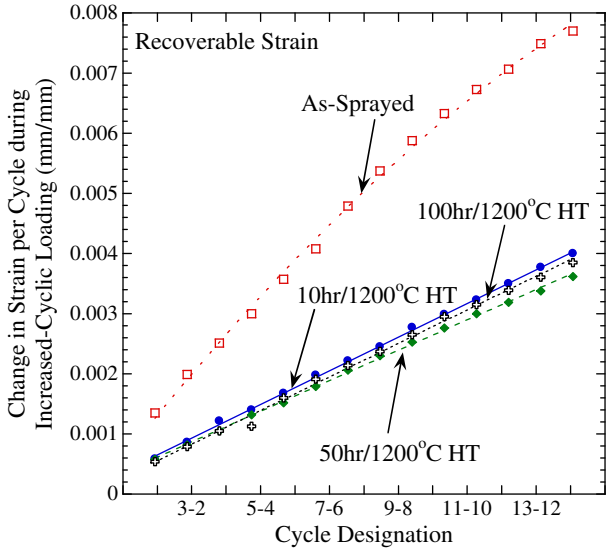

Fig. 6. Recoverable strain per cycle during increased-cyclic loading. All coatings heat-treated at 1200 °C displayed very similar elastic strains throughout the cycling. The lines are added to guide the eyes.

3.4.2. Permanent deformation as a function of increased cyclic loading

The recoverable and permanent strains as a function of loading cycle during increased-cyclic loading are presented in Figs. 6 and 7, respectively, for the as-sprayed samples and heat-treated samples. The recoverable strains as a function of cycle number are linear, with some deviation from linearity noted in the as-sprayed coatings at higher stresses. A comparison of the two figures indicates that the

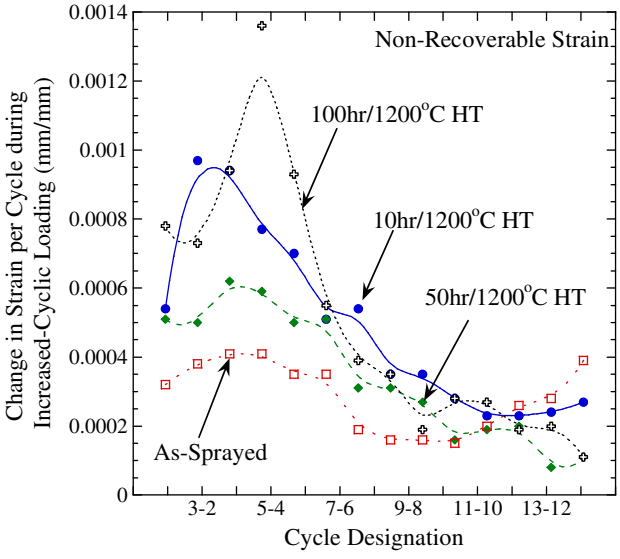

Fig. 7. Permanent strain per cycle during increased-cyclic loading. All coating conditions show a similar trend in permanent strain during loading, where the initial increase in magnitude is believed to be linked to crack growth and lamella sliding during the m_{o1} stage, and the decrease in non-recoverable strain is believed to be linked to a more uniformly distributed load during the m_{o2} stage. The increase in non-recoverable strain during the final cycles of the as-sprayed condition is believed to be linked to increased crack growth and linkage. The line is added to guide the eyes.

recoverable strains are generally larger than the non-recoverable strains, independent of coating condition. For example, in the as-sprayed coating the recoverable strain between cycles 10 and 11 was 0.006 while the non-recoverable strain was 0.0002.

Fig. 6 also shows that the as-sprayed coatings exhibit larger recoverable strain than the heat-treated coatings. This is due to the smaller modulus values noted for the as-sprayed coatings compared to the heat-treated coatings as shown in Fig. 4a, b, and c. Despite lower elastic strains, the heat-treated coatings demonstrate higher permanent strains than the as-sprayed coatings (see Fig. 7), particularly at the lower number of cycles. Thus, it is clear that the heat-treatments tend to decrease the strain tolerance of the sample. Fig. 7 shows a decrease in magnitude of permanent strain at higher applied loads suggesting that the coating increasingly resists permanent deformation. As discussed presently, this is due to the stress becoming more uniformly distributed within the coating, and therefore decreasing points of stress concentration. Lower local stresses result in less crack initiation and growth, and less compaction of lamella.

4. Conclusions

The room temperature stress–strain behavior in APS YSZ coatings has been directly measured in uniaxial compression on as-sprayed and coatings heat-treated at 1200 °C for times ranging from 10 to 100 h. Room temperature mechanical testing was conducted to differentiate deformation mechanisms occurring at room temperature where contributions from diffusion-based deformation mechanisms (like creep) are negligible. APS YSZ coatings demonstrated varying modulus behaviors. For stresses below 100 MPa, a modulus of $\approx$20 GPa was noted. Above 120 MPa through failure, a modulus of $\approx$40 GPa was observed. The increase in modulus is due to the closure of cracks oriented perpendicular to the applied stress and permanent sliding of adjacent lamella. No statistical difference in E_{o1} and E_{o2} moduli was noted after heat-treating, but the relative reloading modulus ($m_{e-\#}$) increased significantly from $\approx$35 GPa to 70 GPa after repeated loading. This increase was due to permanent sliding of adjacent lamella.

Cyclic loading of APS YSZ coatings revealed very complex stress–strain behavior. For constant stress cyclic loading, the amount of permanent strain was observed to decrease with each subsequent load application to a minimum value. Clearly, most of the permanent strain is imparted to the coating during the first few loading cycles. With repeated loadings to the same stress less permanent strain is noted. Values of permanent strain for increased cyclically loaded samples were typically highest during the first few loading cycles. Analysis revealed that early loading cycles caused the most rearrangement of the lamella to accommodate the load.

Acknowledgements

Major portions of this research were funded by the National Science Foundation via grant DMR-0134286. Based in part on the thesis submitted by C. Petorak for the Ph.D. Degree in Materials Engineering, Purdue University, West Lafayette, Indiana, 2007.

References

[1] R. McPherson, Surf. Coat. Technol. 39/40 (1989) 173.
[2] R. McPherson, Thin Solid Films 83 (1981) 297.
[3] R.A. Miller, Surf. Coat. Technol. 30 (1) (1987) 1.
[4] R.B. Heimann, Plasma-Spray Coatings: Principles and Applications, Weinheim, New York, 1996.
[5] J. Allen, J. Ilavksy, G.G. Long, J.S. Wallace, C.C. Berndt, H. Herman, Acta Mater. 49 (2001) 1661.
[6] J. Ilavsky, G.G. Long, A.J. Allen, C.C. Berndt, Mater. Sci. Eng. A. 272 (1999) 215.
[7] Thomas Taylor, Thermal Barrier Coatings for Substrates and Process for Producing It, US Patent 5073433 (1991).
[8] H.B. Guo, S. Kuroda, H. Murakami, J. Am. Ceram. Soc. 89 (4) (2006) 1432.
[9] R. Vassen, H.B. Guo, D. Stover, Adv. Ceram. Coat. Ceram. Met. Syst. Ceram. Eng. Sci. Proc. 26 (3) (2005) 37.
[10] C.G. Samis, M.F. Ashby, Acta Metall. 34 (3) (1986) 511.
[11] M.F. Ashby, S.D. Hallam, Acta Metall. 34 (3) (1986) 497.
[12] B. Siebert, C. Funke, R. Vaben, D. Stover, J. Mater. Process. Technol. 92–93 (1999) 217.
[13] S.R. Choi, D. Zhu, R.A. Miller, Ceram. Eng. Sci. Proc. 19 (4) (1998) 293.
[14] J.P. Levin, G.R. Dickinson, R.W. Trice, J. Am. Ceram. Soc. 87 (5) (2004) 960.
[15] H. Gao, "The Deformation and Fracture of Thick Thermal Barrier Coatings," Ph.D. Thesis, University of Illinois at Urbana-Champaign, (2003).
[16] S.R. Choi, D. Zhu, R.A. Miller, J. Am. Ceram. Soc. 20 (3) (1999) 365.
[17] Y. Liu, T. Nakamura, G. Dwivedi, A. Valarezo, S. Sampath, J. Am. Ceram. Soc. 91 (12) (2008) 4036.
[18] Y. Liu, T. Nakamura, V. Srinivasan, A. Vaidya, A. Gouldstone, S. Sampath, Acta Mater. 55 (2007) 4667.
[19] R.W. Trice, Y.J. Su, J.R. Mawdsley, K.T. Faber, A.R. De Arellano-López, H. Wang, W.D. Porter, J. Mater. Sci. 37 (2002) 2359.
[20] J.A. Thompson, T.W. Clyne, Acta Mater. 49 (2001) 1565.
[21] K.F. Wesling, D.F. Socie, B. Beardsley, J. Am. Ceram. Soc. 77 (7) (1994) 1863.
[22] K. Erk, C. Deschaseaux, R. Trice, J. Am. Ceram. Soc. 89 (5) (2006) 1673.
[23] W.W. Mullins, J. Appl. Phys. 28 (3) (1957) 333.
[24] W.W. Mullins, AIME Trans. 218 (1960) 354.
[25] D. Zhu, R.A. Miller, J. Mater. Res. 14 (1) (1999) 146.
[26] Petorak, "Evolution of the Plasma-Sprayed Microstructure in 7 wt% Yttria-Stabilized Zirconia Thermal Barrier Coatings during Uniaxial Stress Relaxation and the Concomitant Changes in Material Properties," PhD. MSE Thesis, Purdue University (2007).
[27] E. Withey, C. Petorak, R. Trice, G. Dickinson, T. Taylor, J. Eur. Ceram. Soc. 27 (2007) 4675.
[28] G.R. Dickinson, C. Petorak, K. Bowman, R. Trice, J. Am. Ceram. Soc. 88 (8) (2005) 2202.
[29] J.B. Wachtman, Mechanical Properties of Ceramics, 1st Ed., Wiley, New York, 1996, p. 392.
[30] J. Wachtman, Mechanical Properties of Ceramics, Wiley-Interscience, 1996, p. 392.
[31] R. Stevens, An Introduction to Zirconia, 2nd Ed., MEL, Manchester, 1986.
[32] A. Selcuk, A. Atkinson, J. Eur. Ceram. Soc. 17 (1997) 1523.
[33] S.R. Choi, D. Zhu, R.A. Miller, Int. J. Appl. Ceram. Technol. 1 (4) (2004) 330.
[34] A. Selcuk, A. Atkinson, J. Eur. Ceram. Soc. 17 (1997) 1523.
[35] J.A. Thompson, T.W. Clyne, Acta Mater. 49 (2001) 1565.
[36] A. Atkinson, A. Selcuk, Solid State Ionics 134 (2000) 59.